

Supporting Information for:

Zero Volt Paper Spray Ionization and its Mechanism

Michael Wleklinski,^{1#} Yafeng Li,^{1#} Soumabha Bag,¹ Depanjan Sarkar,² Rahul Narayanan,² T. Pradeep² and R. Graham Cooks^{1*}

¹Department of Chemistry and Center for Analytical Instrumentation Development, Purdue University, West Lafayette, Indiana 47907

²DST Unit of Nanoscience (DST UNS) and Thematic Unit of Excellence (TUE), Department of Chemistry, Indian Institute of Technology Madras, Chennai 600 036, India

* Corresponding Author: cooks@purdue.edu

These authors contributed equally

Keywords: Ambient Ionization; Charged Droplets; Inlet Ionization; Nanoelectrospray; Charge Residue Model; Electrospray Mechanism; Acid/Base Equilibria; Surface Activity; Coulombic Repulsion; Aerodynamic Breakup; Asymmetric Charge Distribution

Abstract: The supporting information includes 11 figures, 4 movies, and further simulation details. Figure S1 shows the process of one droplet being sucked into the mass spectrometer. Figures S2 and S3 display MS/MS data for selected analytes examined in the positive and negative ion modes ionized by paper spray (PS), nano-electrospray ionization (nESI), and zero volt PS. Figures S8 – S10 are supporting information for the simulations developed in this paper. A in depth discussion of the postulated ionization mechanism for zero volt paper spray is provided. A brief discussion of figure S11 is also provided.

Supplementary Figures:

Figure S1: Consecutive camera images of 0V paper spray process.

Figure S2: MS/MS of selected positive mode analytes using PS, nESI, and zero volt PS

Figure S3: MS/MS of selected negative ion mode analytes using PS, nESI, and zero volt PS

Figure S4: 0V paper spray of aromatic heterocycles in neutral and acidic pH

Figure S5: 0V paper spray of amines with different basicities

Figure S6: Comparison of 0 V and 1 V paper spray

Figure S7: Analysis of mixtures selected compounds using nESI, PS, and zero volt PS.

Figure S8: Weber number for methanol droplets under different gas flows

Figure S9: Simulated number of molecules ionized vs analyte concentration at various surface activities

Figure S10: Simulated ionization efficiency vs analyte concentration at various surface activities

Figure S11: Experimental results of binary mixtures and calculated relative surface activity results.

Supplementary Movies:

Movie S1: Video image of the analysis of 50 ppm tributylamine in methanol feed continuously onto the paper at 15 $\mu\text{L}/\text{min}$.

Movie S2: Video image of the analysis of 50 ppm tributylamine in methanol feed continuously onto the paper at 15 $\mu\text{L}/\text{min}$ at $\frac{1}{4}$ speed.

Movie S3: Video image of the analysis of 50 ppm tributylamine in methanol added in 5-7 μL aliquots.

Movie S4: Video image of the analysis of 50 ppm tributylamine in methanol added in 5-7 μL aliquots at $\frac{1}{4}$ speed.

Additional Experimental Details

Chemicals and Materials

Diphenylamine and adenine were purchased from Merck Ltd., Mumbai, India. Guanine was purchased from Spectrochem Pvt. Ltd., Mumbai, India. Diisopropylamine and methylamine were purchased from SD Fine Chem. Ltd, Mumbai, India. Thymine was purchased from Titan Biotech LTD., New Delhi, India. Pyridine was purchased from Qualigens Fine Chemicals, India. Tetramethyl-1,4-butanediamine was purchased from Sigma Aldrich, India. All compounds purchased in India were dissolved in HPLC grade methanol (Sigma Aldrich, India). All other samples were purchased from Sigma (St. Louis, MO, USA).

Additional Simulation Details

Aerodynamic Breakup

When sufficient solvent is applied, droplets are pulled from the filter paper by the suction of the instrument. Typically a few μL of sample is added before each suction event suggesting that the initial droplets will be at least of similar volume. The droplets, initially at zero velocity enter a high speed gas flow (170 m/s) due to the suction of the inlet and experience an aerodynamic force.³ This force causes the droplet to simultaneously accelerate and breakup. The droplet will continue to breakup while its Weber number is larger than 10.^{4,5} The weber number is defined by

$$We = \frac{\rho_g (V_g - V_d)^2 D_d}{\sigma} \quad (1)$$

where ρ_g is the gas density, V_g is the gas velocity, V_d is the droplet velocity, D_d is the diameter of the droplet, and σ is the surface tension of the solvent.⁴ This suggests that droplets will primarily breakup due to aerodynamic forces until they either accelerate to the velocity of the surrounding gas or reach a certain size. There is evidence from charge detection mass spectrometry that water droplets produced by either sonic spray ionization or vibrating orifice aerosol generator reach a common size of about 2.5 μm after traveling through the inlet.⁵ This is also approximately the average size measured for kV PS mass spectrometry.⁶ This suggests that methanol droplets should undergo a similar phenomenon, but in fact could be smaller due to the reduced surface tension of methanol as compared to water. Using this information, it is assumed that droplets may have diameters between 1-4 μm after aerodynamic breakup (Figure S8).

Initial Droplet Conditions for Evaporation and Columbic Fission Cycles

Aerodynamic breakup determines that droplets will have diameters between 1 and 4 μm and this serves as the initial diameter of droplets modeled in this section. The number of analytes in a droplet was calculated based on initial analyte concentration and its dissociation constant to determine the number of ions it will produce. Only ions can be separated into detectable quantities by mass spectrometry, thus solution phase neutrals are ignored in this model. The initial droplet charge was

modeled by the statistical fluctuations of positive and negative ions present in the total population of ions. For a droplet containing n ions, of which the ions are either positively or negatively charged, the overall charge is modeled by a binomial distribution (2).

$$f(z; n, p) = \binom{n}{z} p^z (1 - p)^{n-z} \quad (2)$$

For this distribution, p is the probability of an ion being charged (either positive or negative), n is the number of ions, and z is number of positive charges. The initial number of positive and negative ions is on average, equal; however, statistical fluctuations in the positive and negative ions will produce some net charge. This is simulated by using a binomial random number generator with parameter $p = 0.5$ and n is the previously calculated number of ions. The initial charge is found by subtracting the number of negative ions from the positive ions.

Droplet Evaporation to Rayleigh Limit

With the droplet's initial parameter set (size, charge, number of analytes), evaporation is allowed to occur. The temperature of the droplet was kept constant at 298 K to ease the computation time required. This is justified by the fact that droplets will cool evaporatively,⁷ but will also be warmed by collisional activation, so the temperature will drop initially but may rise later on, thus an accurate model for temperature will be difficult to obtain over the droplet size range of the simulation (4 μm – 10 nm).⁸⁻¹⁰ The droplet is allowed to evaporate until it reaches the Rayleigh limit diameter.^{11,12}

$$D_R = \left(\frac{D_q^2 * e^2}{(\pi^2 * 8 * \epsilon_0 * \gamma)} \right)^{\frac{1}{3}} \quad (3)$$

Here D_q is the charge on the droplet, e is elementary charge, ϵ_0 is the permittivity of a vacuum, and γ is the solvent surface tension. Surface tension was estimated using a regression method developed by Jasper et al.^{13,14}

Droplet Fission and Progeny Droplets

Upon reaching the Rayleigh limit, droplets undergo fission and lose mass and charge in the form of progeny droplets. At this point columbic fission occurs with most reports indicating a small mass loss, Δm , (2%) from the precursor droplet and large charge loss, Δq , (15%).¹⁵⁻¹⁷ From this the diameter of the precursor and progeny droplets can be calculated, assuming that on average 10 progeny droplets are generated in a fission event. The exact number of progeny droplets generated is unknown, but 10 is within the range of typical values reported.¹⁸⁻²⁰ Accordingly the size of precursor and progeny droplets was calculated according to these equations:

$$D_d = (1 - \Delta m)^{\frac{1}{3}} * D_R \quad (4)$$

$$D_{pD} = \left(\frac{\Delta m}{N_{pd}} \right)^{\frac{1}{3}} D_R \quad (5)$$

where N_{pd} is the number of progeny droplets taken to be 10, D_{pd} is the diameter of the progeny droplets, and $\Delta m = 0.02$. At the time of fission only ions that are close to the surface are allowed the possibility of being transferred to a progeny droplet. A volume fraction, V_f , is specified as the volume which can be considered for transfer to progeny droplets. In this simulation it is taken to be 15% of the total volume, but the exact value is unknown. The position of a solvated ion within a droplet is determined by its surface activity, S . Surface activity is a number between 0 and 1 describing the probability of a molecule being at the surface or the interior of the droplet. This is modeled by a binomial distribution, similar to equation (2), except that $p = S$, n is the number of ions, and z is the number of ions found in the outer region of the droplet. Thus when $S = 1$ all ions are located in the outer region, and when $S = 0$, none are located in the outer region. Any ions free of their respective counter charge are assumed to be in the outer region of the droplet. The average number of ions, N_{IP} , and charges, N_q , per progeny droplet are calculated from (6) and (7)

$$N_{IP} = \left(\frac{D_d}{D_{pd}} \right)^3 * V_f * C_{IP} \quad (6)$$

$$N_q = \frac{C_q * \Delta q}{N_{pd}} \quad (7)$$

where C_{IP} and C_q are the number concentration of ions and charges in the outer region of the droplet. The number of ions transferred to progeny droplets can be modeled by a Poisson distribution.²¹ The number of ions, $N_{anal-IP}$, and charges, N_{anal-q} is chosen randomly from a Poisson distribution.

$$f(N_{anal-IP}, N_{IP}) = \frac{e^{-N_{IP}} * N_{IP}^{N_{anal-IP}}}{N_{anal-IP}!} \quad (8)$$

The same equation is used for N_{anal-q} with the appropriate substitutions. At this point, more random charging can occur due to the statistical fluctuations of positive and negative ions present in the total population of positive and negative ions. This is modeled in the same manner as described in the initial droplet conditions section (equation 2). With this information, the charge of the progeny droplet is calculated by subtracting the total population of positive ions from negative ions. This same methodology is completed for all the other progeny droplets, and then the conditions of the precursor droplet are updated based on the total number of ions consumed by the progeny droplets. All droplets (precursor and progeny) larger than 10 nm then undergo more evaporation/fission cycles until all droplets reach 10 nm in size.

Analyte Ion Formation

Once all droplets have reached 10 nm in size the simulation ends. At this time each droplet is analyzed for charge to determine the number of ionized analytes. For example, a droplet containing a +2 charge is assumed to have two ionized molecules. Note that in the simulation the actual ionization event is not modeled explicitly. Gas phase ions could be produced by either the charge residue model or the ion evaporation model. This counting process is repeated for all the droplets of size <10 nm and then ionization efficiency can be calculated. Typically 5,000 – 50,000 precursor droplets are modeled to obtain an estimate of ionization efficiency and total number of ionized molecules. Alternatively this model can be applied to droplets containing multiple analytes, in which case multiple analyte ratios can be calculated. Note that multiple charges on the small analytes of interest are very unlikely and this possibility is ignored.

Experimental and Simulated Results and Mechanistic Considerations for Multi-Analyte Mixtures

In Figure S11a, the amount of tetrabutylammonium iodide was held constant at 0.1 ppm, while that of cocaine was changed. In Figure S11a the ratio of cocaine to tetrabutylammonium iodide increases as the concentration of cocaine increases. Figure S11b shows a similar trend to Figure 5b, but since the amount of cocaine is increased the calculated relative surface activity of cocaine increases. Again this is because as the cocaine concentration increases, more cocaine can occupy the surface increasing its relative surface activity. In Figure S11c, sodium tetraphenylborate was held constant at 5 ppm and 3,5-dinitrobenzoic acid was varied. The data in Figure S11c are consistent with those of Figure S11a in that as the concentration of the analyte increases the ratio of analyte to salt signal increases. Additionally the relative surface activity of 3,5-dinitrobenzoic acid increases (Figure S11d) as the analyte concentration increases. The only noticeable difference is in the nESI results of Figure S11c, which show a drop in the ratio of 3,5-dinitrobenzoic acid to sodium tetraphenylborate in spite of its higher surface activity.

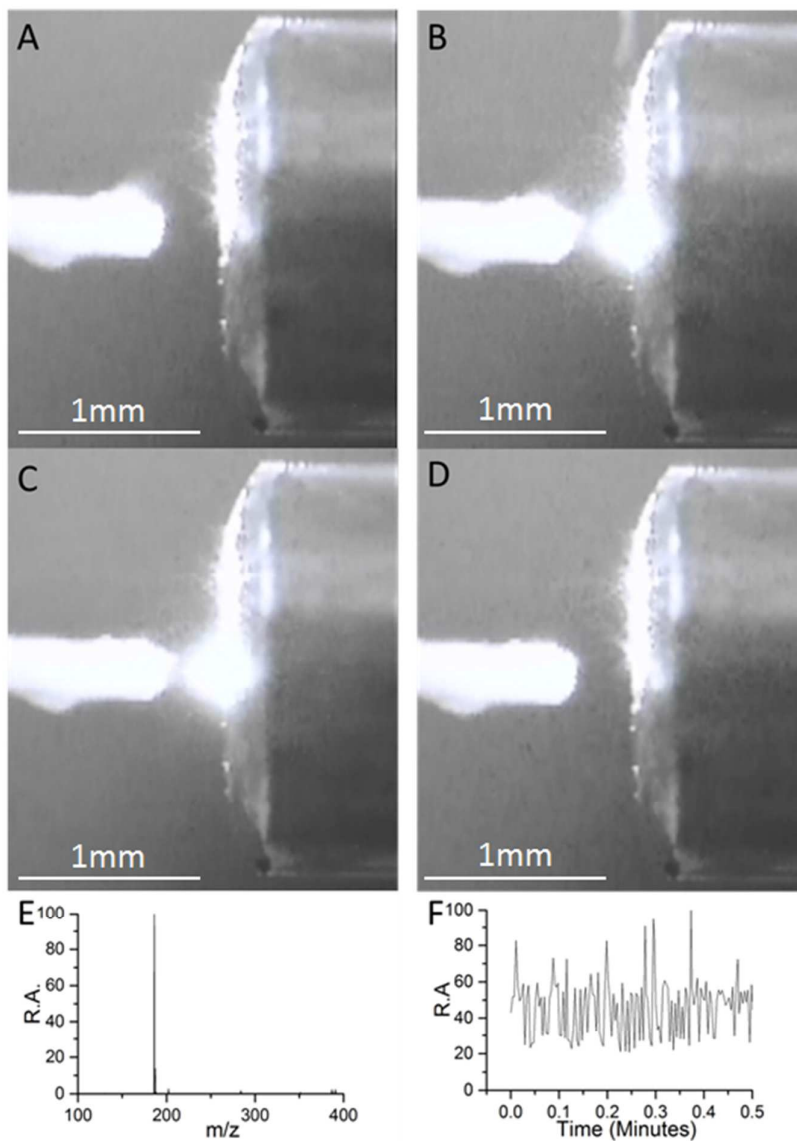


Figure S1. Panels A-D are consecutive images of the spray process occurring at 0 volts. The spray is illuminated with a red laser pointer and captured on a Watec Wat-704R camera. Panels A-D show a droplet event over the course of 4 consecutive scans. The time elapsed is around 100 milliseconds. Panels E and F are the mass spectrum of 50 ppm tributylamine and its corresponding ion chromatogram. Tributylamine was added in a continuous manner at 15 $\mu\text{L}/\text{min}$ through a fused silica capillary.

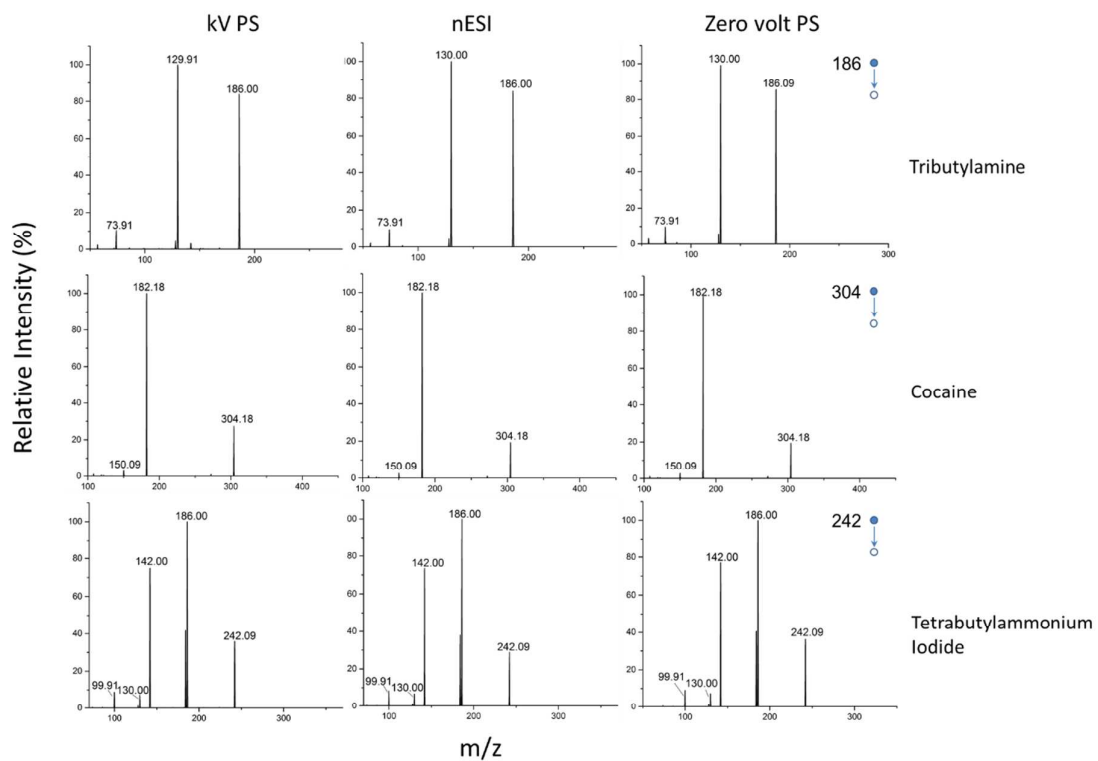


Figure S2. Positive ion mode MS/MS data for tributylamine, cocaine, and tetrabutylammonium iodide taken by kV paper spray, nano-electrospray ionization, and zero volt paper spray.

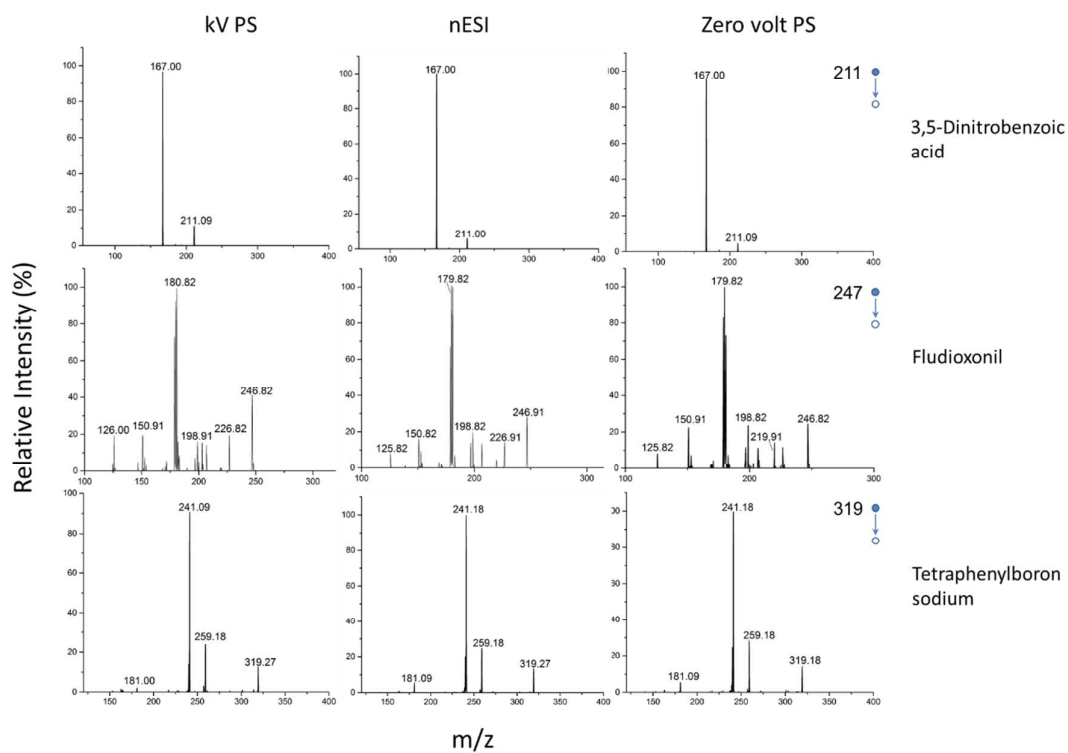


Figure S3: Negative ion mode MS/MS data for 3,5-dinitrobenzoic acid, fludioxonil, and sodium tetraphenylborate taken by kV paper spray, nano-electrospray ionization, and zero volt paper spray.

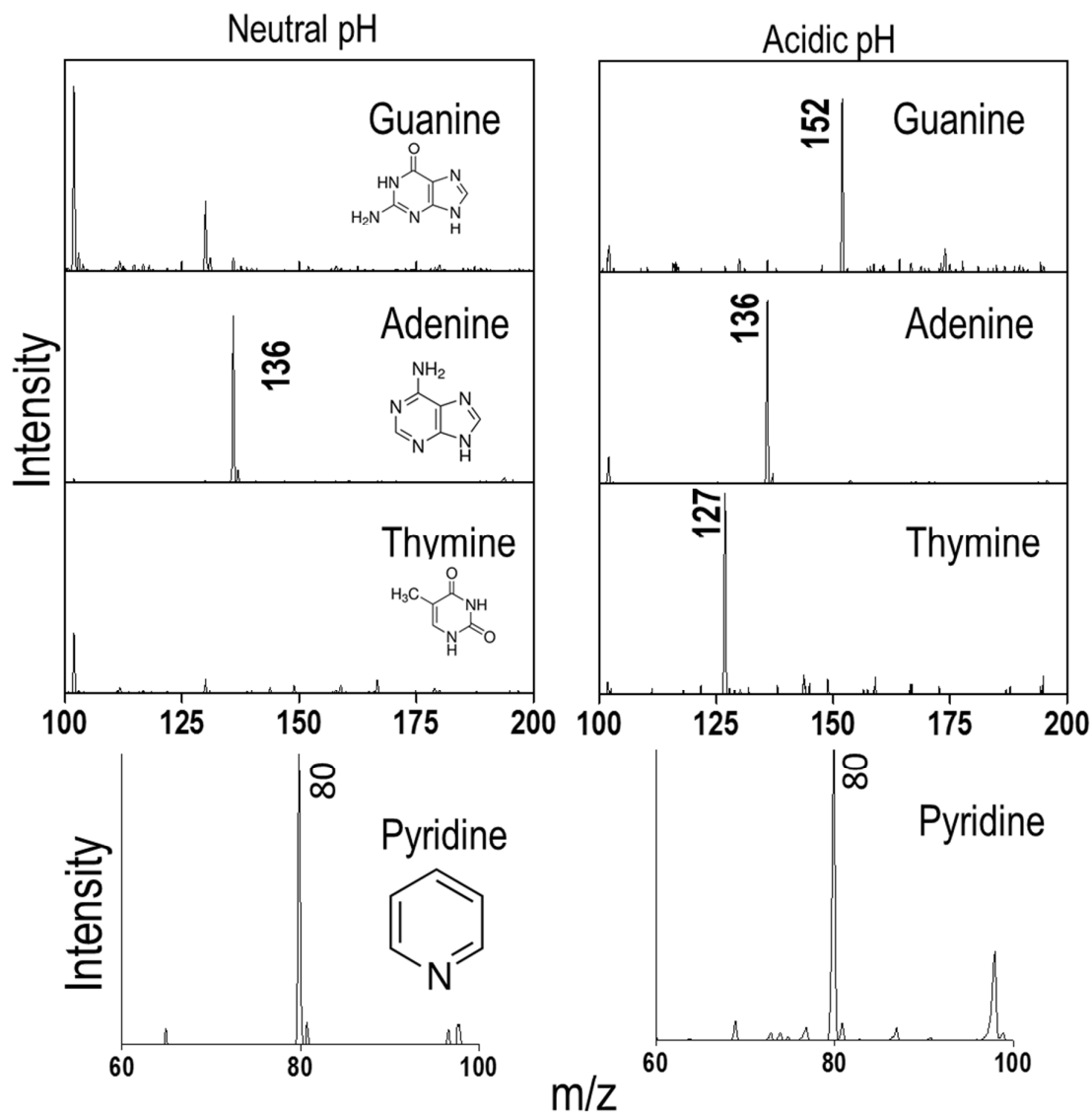


Figure S4: Analysis of aromatic heterocycles, guanine (top, m/z 152), adenine (middle, m/z 136), thymine (middle, m/z 127), and Pyridine (bottom, m/z 80) with 0 V paper spray under both neutral (left) and acidic conditions (right).

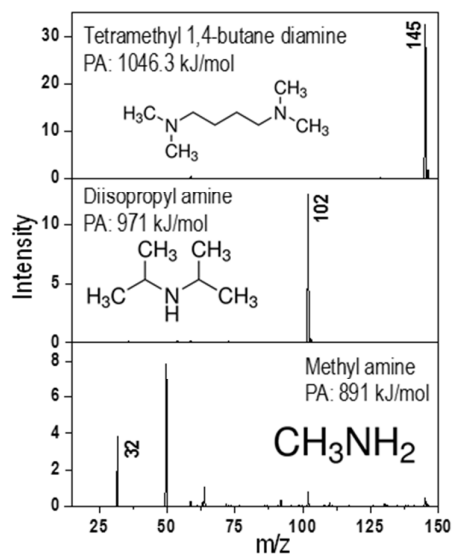


Figure S5: Analysis of three different amines. Tetramethyl-1,4-butanediamine (top, m/z 145), diisopropylamine (middle, m/z 102), and methyl amine (bottom, m/z 32). All samples are dissolved in methanol at neutral with pH 7. Proton affinities are obtained from NIST Webbook.

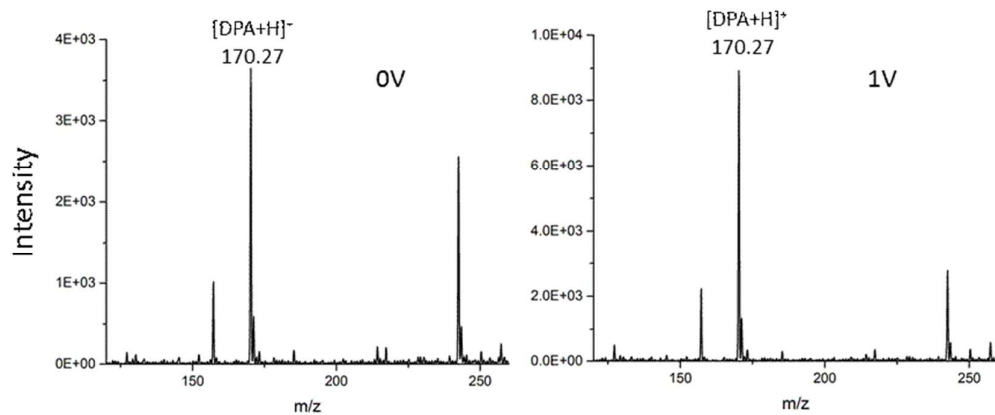


Figure S6: Mass spectra of 50 ppm diphenylamine (DPA) on a paper substrate at 0 V and 1 V, respectively. Note the difference in scales and the fact that the m/z 170 signal intensity is about 1.5 times higher than that at 0 V.

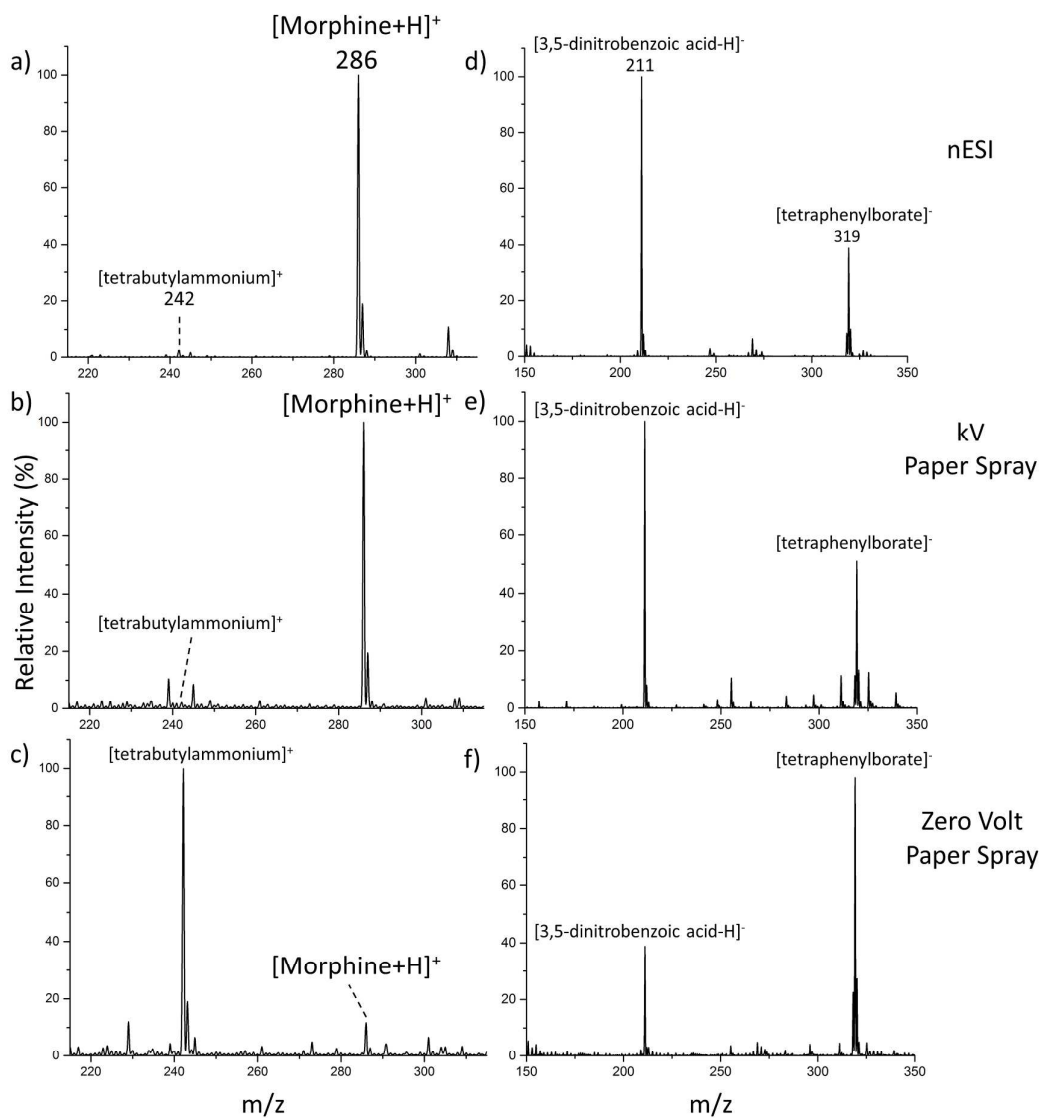


Figure S7: Mass spectra of 5 μ L of a mixture of 9 ppm morphine and 0.1 ppm tetrabutylammoniumiodide using a) nESI, b) kV PS, and c) zero volt PS. Mass spectra of 5 μ L of a mixture of 36 ppm 3,5-dinitrobenzoic acid and 5 ppm sodium tetraphenylborate using d) nESI, e) kV PS, and f) zero volt PS. The relative intensity of tetrabutylammonium signal to morphine in zero volt PS is much higher than in nESI and kV PS in both cases. The same is true of the ratio of tetraphenylborate to 3,5-dinitrobenzoic acid for zero volt PS as compared to nESI and kV PS.

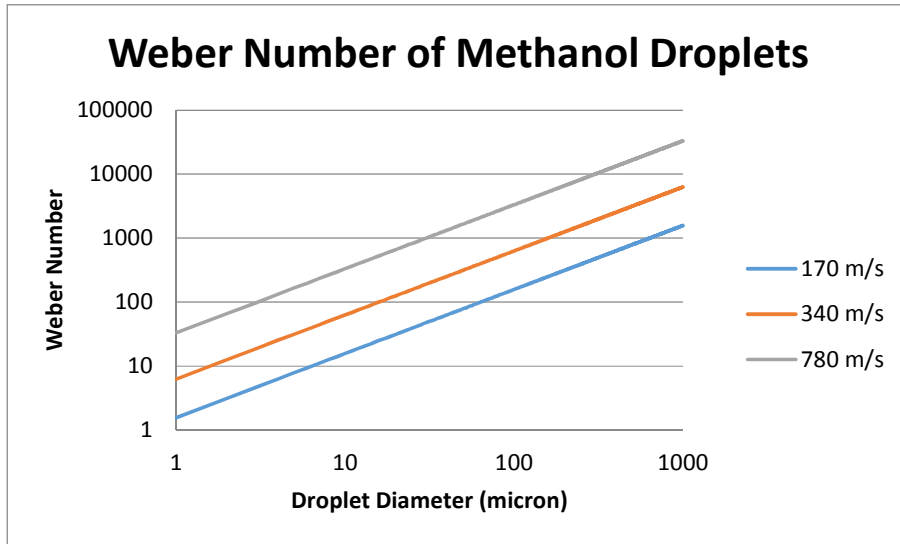


Figure S8. Simulation results of Weber number of methanol droplets. Using this information, it is assumed that droplets may have diameters between 1-4 μm after aerodynamic breakup.

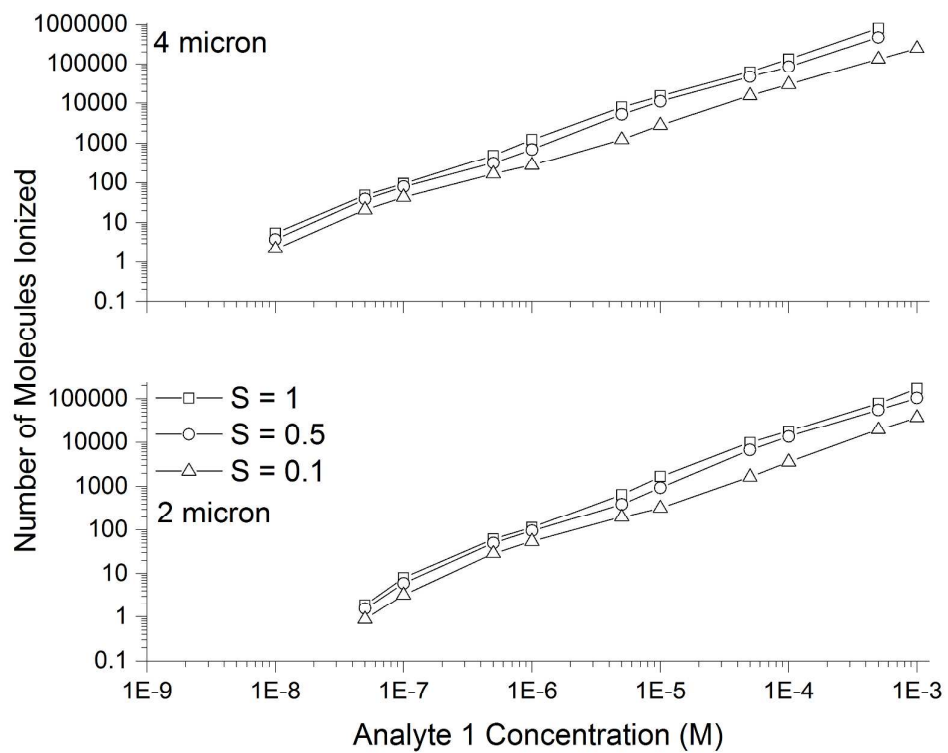


Figure S9. The number of ionized molecules vs. concentration for 2 micron (bottom) and 4 micron (top) droplets. The simulation was run at three different surface activities.

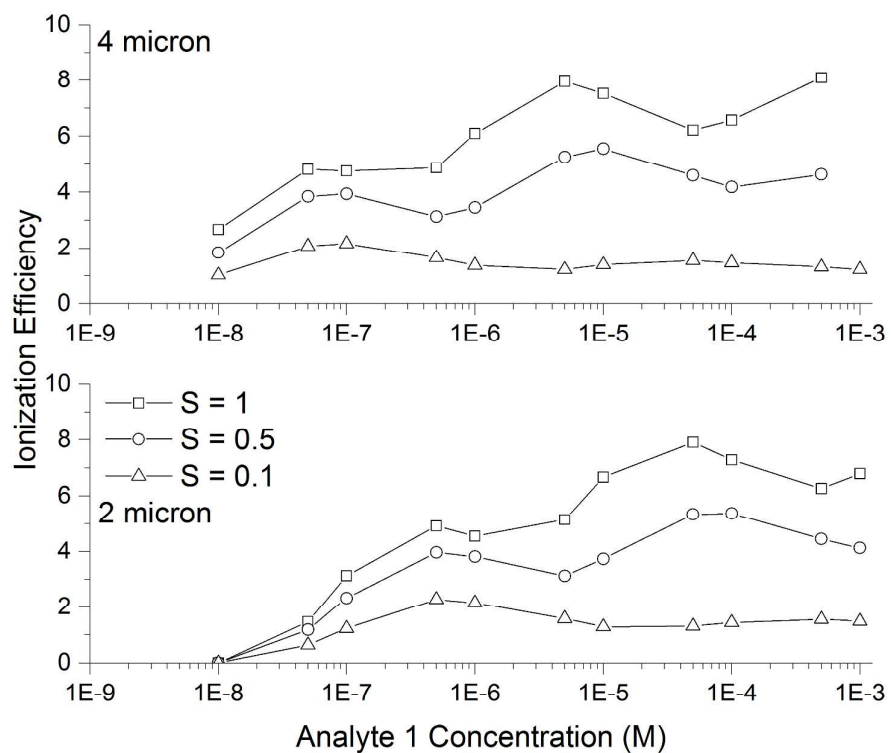


Figure S10. Ionization efficiency vs. concentration of 2 micron (bottom) and 4 micron (top) droplets. The simulation was run at three different surface activities.

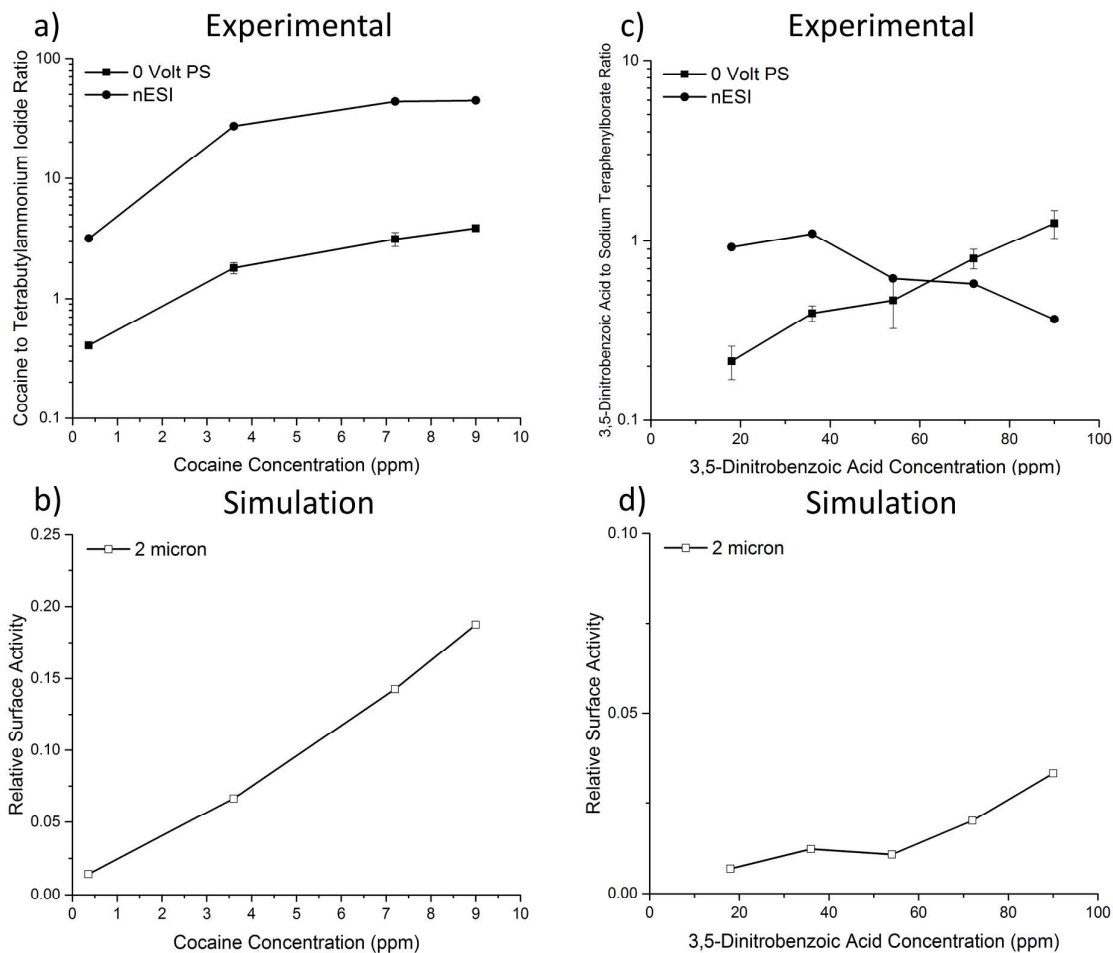


Figure S11. Cocaine to tetrabutylammonium iodide ratio dependence in positive ion mode for zero volt PS and nESI. a) Tetrabutylammonium iodide concentration is held constant at 0.1 ppm, while cocaine concentration changes. b) Relative surface activity of cocaine calculated to match the experimental ratio in part a). c) Sodium tetrphenylborate is held constant at 5 ppm, while 3,5-dinitrobenzoic acid concentration changes. d) Relative surface activity of 3,5-dinitrobenzoic acid calculated to fit experimental data in part c). Surface activity of the salt is assumed to be 1 for simulations.

Supplementary Movies:**Movie Captions:**

Supplementary Movie 1: This movie shows the analysis of 50 ppm tributylamine with zero volt paper spray. Continuous feeding at 15 $\mu\text{L}/\text{min}$ is used to feed the paper. With continuous feeding, a near continuous stream of droplets is observed entering the mass spectrometer inlet.

Supplementary Movie 2: Same as supplementary movie 1 but at $\frac{1}{4}$ speed.

Supplementary Movie 3: This movie shows the analysis of 50 ppm tributylamine with zero volt paper spray. Seven μL aliquot additions are added to the paper to cause generation of droplets. When solvent is added a group of droplet can be seen entering the mass spectrometer inlet.

Supplementary Movie 4: Same as supplementary movie 3 but at $\frac{1}{4}$ speed.

References:

- (1) Qian, H.-S.; Yu, S.-H.; Gong, J.-Y.; Luo, L.-B.; Fei, L.-f. *Langmuir* 2006, 22, 3830-3835.
- (2) Moon, G. D.; Lee, T. I.; Kim, B.; Chae, G.; Kim, J.; Kim, S.; Myoung, J.-M.; Jeong, U. *ACS Nano* 2011, 5, 8600-8612.
- (3) Zilch, L. W.; Maze, J. T.; Smith, J. W.; Ewing, G. E.; Jarrold, M. F. *The Journal of Physical Chemistry A* 2008, 112, 13352-13363.
- (4) Krzeczowski, S. A. *International Journal of Multiphase Flow* 1980, 6, 227-239.
- (5) Wierzba, A. *Experiments in Fluids* 1990, 9, 59-64.
- (6) Espy, R. D.; Muliadi, A. R.; Ouyang, Z.; Cooks, R. G. *International Journal of Mass Spectrometry* 2012, 325-327, 167-171.
- (7) Gibson, S. C.; Feigerle, C. S.; Cook, K. D. *Analytical Chemistry* 2013, 86, 464-472.
- (8) Merenbloom, S.; Flick, T.; Williams, E. J. *Am. Soc. Mass Spectrom.* 2012, 23, 553-562.
- (9) Konermann, L.; McAllister, R. G.; Metwally, H. *The Journal of Physical Chemistry B* 2014, 118, 12025-12033.
- (10) Gabelica, V.; Pauw, E. D. *Mass Spectrometry Reviews* 2005, 24, 566-587.
- (11) Rayleigh, L. *Philosophical Magazine Series 5* 1882, 14, 184-186.
- (12) Kebarle, P.; Verkerk, U. H. *Mass Spectrometry Reviews* 2009, 28, 898-917.
- (13) Lange, N. A.; Speight, J. G. *Lange's handbook of chemistry*, 16th ed.; McGraw-Hill: New York, 2005.
- (14) Jasper, J. J. *Journal of Physical and Chemical Reference Data* 1972, 1, 841-1010.
- (15) Fernández de la Mora, J. *Journal of Colloid and Interface Science* 1996, 178, 209-218.
- (16) Tang, K.; Smith, R. D. *International Journal of Mass Spectrometry* 1999, 185-187, 97-105.
- (17) Cech, N. B.; Enke, C. G. *Analytical Chemistry* 2001, 73, 4632-4639.
- (18) Chen, D.-R.; Pui, D. Y. H.; Kaufman, S. L. *Journal of Aerosol Science* 1995, 26, 963-977.
- (19) Konermann, L. *J. Am. Soc. Mass Spectrom.* 2009, 20, 496-506.
- (20) Kebarle, P.; Tang, L. *Analytical Chemistry* 1993, 65, 972A-986A.
- (21) Hogan Jr, C. J.; Biswas, P. *J. Am. Soc. Mass Spectrom.* 2008, 19, 1098-1107.